RSC Advances

PAPER

View Article Online
View Journal | View Issue

Cite this: *RSC Adv.*, 2024, **14**, 12935

Wet adhesive hydrogels based on niobium carbide for experimental research of oral mucosal impairment†

Jiayuan Chen, ‡[a] Junyu Ren,‡[b] Yingjie Wu, [c] Narisu Hu,*[b] Fang Zhao*[d] and Lin Zhang*[a]

Received 22nd February 2024
Accepted 13th April 2024

DOI: 10.1039/d4ra01352b

rsc.li/rsc-advances

Oral mucosal impairment is a prevalent oral disease that frequently causes pain for patients. Conventional treatments have limited effectiveness and can cause adverse reactions. Furthermore, the moist and dynamic nature of the oral mucosal environment makes persistent adherence of conventional materials challenging, which can affect treatment efficacy. In this study, we investigated the potential of a NbC/TA–GelMA hydrogel system, where niobium carbide (NbC) and tannic acid (TA) were added to gelatin methacryloyl (GelMA), for repairing oral mucosal impairment. The wet adhesion properties of NbC/TA–GelMA hydrogels were confirmed by the inclusion of TA with a catechol-rich group. In addition, the photothermal effect of NbC/TA–GelMA hydrogel under near-infrared light, synergizing with TA, provided sustained antibacterial action. Furthermore, the NbC/TA–GelMA hydrogel effectively healed damaged oral mucosa of rats.

1 Introduction

Oral mucosal impairments are common lesions of the oral cavity that occur after the oral mucosa is exposed to external stimuli or injury.[1] Common oral mucosal impairments include oral ulcers, gingivitis, and oral mucositis, which negatively impact patients' daily lives and reduce quality of life.[2–4] If left untreated, oral mucosal impairment can progress to severe disease.[5,6] Oral mucosal impairments frequently manifest as the breakdown of the oral mucosa and destruction of connective tissue,[7] local bleeding, bacterial infections, inflammation, and other related complications, which often cause significant pain and discomfort for patients.[1,8,9] The presence of large numbers of bacteria in the oral cavity can hinder the healing process of oral mucosal impairment by impeding the formation of oral epithelium.[10] Oral mucosal impairments are often accompanied by bleeding, and nutrient-rich blood serves as a culture medium for bacteria. Therefore, topical anti-bacterial treatments are crucial in promoting healing of oral mucosal impairment.[11–14] Inappropriate use of antibiotics can cause bacterial resistance, which has become a serious global problem,[15,16] limiting the pharmacological treatment of oral mucosal impairment.[17–20]

Conventional treatments for oral mucosal impairment include antibacterial mouthwashes, antibiotic ointments, oral rinses or sprays, fibrin gels, and glucocorticoid patches. However, these methods have certain disadvantages; for example, mucosal patches can be uncomfortable when applied,[21] and ointments and gels lack a comprehensive therapeutic effect although they are more comfortable in dosage form.[22,23] In recent years, many scholars have made improvements to these methods. For example, H. E. *et al.*[24] prepared electrospun patches that could continuously release loaded drugs in the oral cavity; M. M. *et al.*[25] developed nanofiber membranes based on poly(ε-caprolactone) for periodontal tissue regeneration; S. K. *et al.*[26] presented adhesive nanofiber membranes composed of chitosan and pectin derivatives, and the results showed that they could adhere well to the oral mucosa. Hydrogels have been widely used as wound dressings owing to their elasticity, wettability, and good biocompatibility. Polymer-based hydrogels such as chitosan, gelatin, and polyvinyl alcohol have been used as therapeutic materials for treating oral mucosal impairment.[1,8,27,28] However, these hydrogels each have limitations leading to constraints in their application for oral mucosal impairments. Table 1 summarizes the advantages and disadvantages of some commercially

[a]*First Affiliated Hospital of Harbin Medical University, College of Stomatology, Harbin Medical University, No. 143 Yiman Street, Nangang District, Harbin, 150001, China. E-mail: cczhlin@163.com*

[b]*Oral Implant Center, Second Affiliated Hospital of Harbin Medical University, Harbin Medical University, Harbin, Heilongjiang, China. E-mail: hmuhunarisu@163.com*

[c]*Key Laboratory of Microsystems and Microstructures Manufacturing (Ministry of Education), School of Medicine and Health, Harbin Institute of Technology, No. 92 XiDaZhi Street, Harbin, 150001, China*

[d]*Department of Dentistry, Second Affiliated Hospital of Harbin Medical University, Harbin Medical University, Harbin, Heilongjiang, China. E-mail: dentistzhaofang@163.com*

† Electronic supplementary information (ESI) available. See DOI: https://doi.org/10.1039/d4ra01352b

‡ Authors contributed equally.

Table 1 Comparison of different hydrogels[a]

Hydrogels	Advantages	Disadvantages
Bayer gel(M)	Temporary pain relief; good biocompatibility	Short adhesion time; containing alcohol (40%)
Bonjela gel(M)	Temporary pain relief; anti-inflammatory; analgesic drugs; good biocompatibility	Causing allergic reactions; short adhesion time
Olioli gel(M)	Temporary pain relief; good biocompatibility	Short adhesion time; uncomfortable odor; causing allergic reactions
Chlorhexidine hydrogel patch[29]	Anti-bacteria; anti-inflammatory	Pigmentation; short adhesion time; causing allergic reactions
AHPs[30]	Anti-bacteria; anti-inflammatory	Uncertain hemostatic performance; uncertain analgesic effect
PVA-DOPA mucoadhesive film[27]	Good biocompatibility; good adhesion strength	Uncertain anti-bacteria and hemostatic performance; uncertain analgesic effect
Glycol-chitosan-c[31]	Good biocompatibility and hemostatic performance	Uncertain anti-bacterial and hemostatic performance, uncertain adhesion strength; uncertain analgesic effect
NbC/TA–GelMA hydrogel	Good biocompatibility and hemostatic performance; good anti-bacteria and anti-inflammatory performance	Uncertain analgesic effect

[a] M: market selling.

available and previously reported hydrogels compared with the hydrogel in this study.

The temperature and humidity of the oral environment are conducive for bacterial growth. The presence of a large number of bacteria has a significant impact on human health.[32] Bacteria can easily adhere to all surfaces of the oral mucosa, which can make them difficult to remove.[33,34] Antibiotics, glucocorticoids, and other drugs used to treat oral mucosal impairments often contain harmful substances that can cause unhealthy reactions, such as gastrointestinal damage; discoloration, dryness, and sensitivity of the oral mucosa; and taste disorders.[35,36] Therefore, materials for treating oral mucosal impairments should ideally possess excellent biocompatibility, strong anti-inflammatory and antibacterial characteristics, and hemostatic properties to establish an optimal healing microenvironment. In addition, the materials should exhibit strong wet adhesion properties to withstand the humid and dynamic environment of the oral cavity and should promote healing of oral mucosal impairments.

Considering that the improper use of antibiotics can cause problems such as bacterial resistance, this study proposes using photothermal sterilization as an alternative approach, which is highly efficient and reduces bacterial resistance.[37] Near-infrared (NIR) light has applications in many industries and fields,[38] with photothermal sterilization being a key use. Photothermal sterilization utilizes photothermal antibacterial materials to absorb NIR light, generate heat, and thereby eliminate bacteria, demonstrating high efficiency and excellent biocompatibility. Photothermal antibacterial nanomaterials have smaller particle sizes and larger surface areas, allowing the absorption of more light energy and higher photothermal conversion efficiency.[39] In this study, niobium carbide (NbC) was selected as a photothermal material for treating oral mucosal impairments owing to its photothermal antibacterial and proangiogenic properties under NIR light and its capacity to decrease the level of reactive oxygen species and mitigate oxidative stress damage.[40] The highly dynamic and wet environment of the oral mucosa means that materials applied for oral mucosal impairment must have strong adhesion properties to ensure the duration of their activity. Tannic acid (TA) can interact with proteins, causing them to clump and adhere to each other,[41] and it can act as an adhesive agent for the wet oral mucosa, allowing hydrogels containing TA to adhere to the surface of the oral mucosa with greater strength.[42] In addition, TA has anti-inflammatory and astringent effects, shrinking tissues and reducing vascular permeability, which is effective in controlling bleeding and reducing pain. Therefore, TA can aid in reducing the area of impairment and promoting healing during the treatment of oral mucosal impairments.[43] Last but not least, TA has antibacterial properties against *Staphylococcus aureus* and *Escherichia coli*.[44] Typically, photothermal materials alone require temperatures as high as 70 °C to effectively eradicate bacteria. However, such high temperatures can cause considerable harm to the healthy tissue surrounding thermally treated wounds. In contrast, the use of photothermal materials can mitigate damage to surrounding tissues and cells at lower temperatures, such as 48 °C, which unavoidably compromised the antibacterial effect.[45,46] In our study, we can determine the amount of NbC needed to achieve mild photothermal effect through photothermal testing. Therefore, the combined use of NbC's photothermal sterilization and TA's chemical sterilization can achieve the desired antibacterial effect while ensuring minimal damage to surrounding tissues. Gelatin methacryloyl (GelMA) is a modified gelatin grafted with methacrylic anhydride, which can form hydrogels under ultraviolet (UV) irradiation when added photosensitizer (LAP)[47,48] Furthermore, GelMA facilitates cell adhesion and proliferation, and serves as a scaffold for tissue regeneration, playing a critical role in the healing of oral mucosal impairments. Hydrogel, which is extensively employed as a wound dressing, can also function as a drug delivery

system. In this study, the hydrogel we synthesized was utilized as a carrier for TA, enabling a controlled and gradual release of the compound to sustain its antibacterial and anti-inflammatory effects. The NbC/TA–GelMA hydrogels also functioned as an immediate hemostatic agent by adhering to the surface of bleeding oral mucosa to create a favorable microenvironment that promotes oral mucosal healing.

2 Experimental

2.1 Materials

Healthy SD male rats, 7 weeks old, weighing 180–250 g were purchased from the Laboratory Animal Centre of Harbin Medical University. All experimental procedures were conducted in accordance with relevant laws and institutional guidelines, and approval was obtained from the Medical Ethics Committee of Harbin Medical University (Ethical Review Approval No. SYDW2023-103). *E. coli*, *S. aureus*, and human oral keratinocytes (HOK) were obtained from the American Type Culture Collection (ATCC). Hematoxylin–Eosin Staining Kit and Masson Staining Kit were purchased from Beijing Solarbio Science & Technology Co., Ltd. The study equipment included a scanning electron microscope (HITACHI), a microcomputer tensile tester (STS-5000, Xiamen EST Instruments Co., Ltd), a fluorescence microscope (Olympus), and a NIR 808 nm laser (Changchun New Industries Optoelectronic Technology Co., Ltd).

2.2 Preparation of hydrogels

To prepare GelMA, 20 g of gelatin was dissolved in 200 mL of deionized water at 40 °C and then slowly dropped into 12 mL of methacrylic anhydride. The reaction was incubated at 40 °C for 3 h with continuous stirring at 1000 rpm with a magnetic rotor, then 800 mL of deionized water was added to dilute and terminate the reaction. The solution was then packed into a dialysis bag and dialyzed in hot water at 40 °C for 4 days, before being transferred to a Petri dish for cooling. Subsequently, the solution was freeze-dried, yielding a white, spongy solid, which was GelMA. Appropriate amounts of TA solution (2.5%) and NbC nanoparticles were mixed with the GelMA, and then the photosensitizer (LAP) was added to form a hydrogel precursor solution that can be crosslinked by UV irradiation to produce a stable gel structure. Hydrogels synthesized from GelMA are known as GelMA hydrogels, those synthesized by incorporating TA into GelMA are referred to as TA–GelMA hydrogels, and those synthesized by combining TA and NbC with GelMA are denoted as NbC/TA–GelMA hydrogels. Further experiments can be performed by spreading the hydrogel precursor solution into cylindrical molds or the oral mucosal surfaces as needed, and crosslinking under UV irradiation to form hydrogels. The NbC/TA–GelMA hydrogel was characterized using techniques such as scanning electron microscopy (SEM), X-ray diffraction (XRD), and dynamic light scattering.

2.3 Organic adhesion performance test

Owing to the similarity in texture between the surface mucosa of organs and the oral mucosa, we selected organs of rats for experiments evaluating the adhesion properties of the hydrogels. After SD rats were euthanized, their hearts, livers, spleens, and kidneys were extracted. The hydrogel precursor solution was then dispersed onto slides and crosslinked with UV irradiation. The rat organs were expected to be adhered to the slides through the NbC/TA–GelMA hydrogels.

2.4 Lap shear adhesion test

Porcine gingival mucosa (2 cm × 2 cm) was attached to a slide using cyanoacrylate adhesive. The hydrogel precursor solution was then uniformly dispersed on the mucosa to form a hydrogel under UV irradiation. Another slide was covered with hydrogel and then pressurized for 1 minute to fully contact. Finally, it was tested using a microcomputer tensile tester at a constant tensile speed of 1 mm min^{-1}.

2.5 Simulation of the intraoral environment

The hydrogel precursor solution was uniformly dispersed on porcine gingival mucosa and crosslinked to form hydrogels using UV irradiation. The hydrogels were placed in artificial saliva containing 50 mL (37 °C). A magnetic rotor at 1500 rpm was used for agitation, and the number of hydrogels adhered to the mucosa was recorded every 30 min.

2.6 Swelling test of hydrogels

The hydrogels were made using a mold, then were freeze-dried and weighed, recording the weight as W_o. Subsequently, the hydrogels were immersed in artificial saliva. Following dissolution for 1, 2, 3, 4, 5, 6, 8, 12, and 24 h, the hydrogels were weighed as W_t. The swelling ratio (SR) of the hydrogel is calculated using the following formula:

$$\mathrm{SR}\ (\%) = (W_t - W_o)/W_o \times 100\%.$$

2.7 Degradation test of hydrogels

The hydrogel degradation rate was determined by a weight reduction (WR) experiment. The hydrogels were freeze-dried and weighed, recording the weight as W_o. Subsequently, the hydrogels were immersed in artificial saliva for 3, 7, and 14 days, followed by another round of freeze-drying to obtain the final weight, recorded as W_t. The formula for WR is:

$$\mathrm{WR}\ (\%) = (W_t - W_o)/W_o \times 100\%.$$

2.8 Compression test of hydrogels

Hydrogels were made using a mold of cylindrical abrasive (5 mm × 5 mm × 5 mm). Compression tests were then conducted using a microcomputer tensile testing machine with a fixed strain rate of 1 mm min^{-1}.

2.9 TA release experiment of NbC/TA–GelMA hydrogels

Five NbC/TA–GelMA hydrogels were separately soaked in 10 mL-artificial saliva tubes. Subsequently, 2 mL of solution was removed from each tube at 2.5, 5, 7.5, 10, and 12.5 h and the concentration of TA was determined by detecting the optical density at 278 nm (OD278 value). Further tests were also conducted to determine whether NIR irradiation enhanced the release efficiency of TA in hydrogels.

2.10 Hemostatic test

Referring to previous literature, we performed rat tail amputation experiments to verify the hemostatic property of hydrogels.[49] The tail of SD rats was clamped at about 2 cm with a hemostat and amputated. After dropping the hydrogel precursor fluid into the severed tail with a pipette gun and crosslinking it into shape with UV irradiation, the tail was placed on top of filter paper and bleeding was measured after 1 minute. A negative control group of no treatment after tail amputation was included. In addition, ViscoStat Clear, which is commonly used as a hemostatic agent in the oral cavity, was used for a positive control group.

2.11 Visible-NIR absorption test

Aqueous dispersions of NbC nanoparticles with concentrations of 0.125, 0.25, 0.5, and 0.75 mg mL^{-1} and NbC/TA–GelMA hydrogels with 0.125, 0.25, 0.5, and 0.75 mg mL^{-1} concentration of NbC were prepared. Transfer the above samples to cuvettes and performed testing with a wavelength range set from 400 nm to 1300 nm. Record the data and plot the Visible-NIR absorption spectra.

2.12 Photothermal conversion test

Aqueous dispersions of NbC nanoparticles with concentrations of 0.125, 0.25, 0.5, and 0.75 mg mL^{-1} were prepared. Next, a pipette gun was used to transfer 100 μL of the various concentrations of NbC dispersion solutions into a quartz dish. The quartz dish was placed in the center of a NIR light source at a wavelength of 808 nm (1 W cm^{-2}). The solutions were irradiated for 10 min to evaluate the warming effect of NbC and assess its stability. Graphs of the warming curves and five cycles of photothermal temperature increase and decrease were plotted. Because NbC was mixed into hydrogel, we conducted photothermal performance tests on NbC/TA–GelMA hydrogels containing varying concentrations of NbC. Finally, the NbC/TA–GelMA hydrogel with 0.75 mg mL^{-1} concentration of NbC was irradiated for 10 min with a NIR light source at a wavelength of 808 nm (1 W cm^{-2}), and took pictures with an infrared imager every 1 minute.

2.13 Bacterial experimental grouping

In antibacterial experiments, we selected *S. aureus* as a representative Gram-positive bacterium and *E. coli* as a representative Gram-negative bacterium. The experiment was divided into five groups: Control group; NIR group (1 W cm^{-2}; 10 min); GelMA hydrogel group; TA–GelMA hydrogel group; and NbC/TA–GelMA hydrogel (NIR) group, with NbC at 750 μg mL^{-1} based on results of the photothermal performance test. The hydrogel precursor solutions of GelMA hydrogel group, TA–GelMA hydrogel group, and NbC/TA–GelMA hydrogel (NIR) group were placed into cylindrical molds (5 mm × 5 mm × 2 mm) and shaped into hydrogels under UV irradiation. The hydrogels were then separately immersed in bacterial suspension (1×10^7 colony-forming units (CFU) per mL) and co-cultured for 10 min, meanwhile the NbC/TA–GelMA hydrogel (NIR) group received an additional 10 min of NIR irradiation. The bacterial suspension of the Control group was not subjected to any treatment and the bacterial suspension of the NIR group received NIR irradiation for 10 min. Finally, the bacterial suspensions of all groups were cultured for 20 min. All antibacterial experiments were conducted after the above treatments, except for the zone of inhibition assay.

2.14 Live/dead bacteria staining test

The treated bacterial suspensions of all groups were centrifuged, rinsed twice with phosphate-buffered saline (PBS), stained using Calcein-AM and propidium iodide, and observed by fluorescence microscopy. Live bacteria exhibit green fluorescence and dead bacteria exhibit red fluorescence.

2.15 SEM examination of bacteria test

The treated bacterial suspensions of all groups were centrifuged, fixed with 2.5% glutaraldehyde, and dehydrated at different concentrations of ethanol (30, 50, 70, 80, 90, and 100%) for 15 min each time. Subsequently, the bacterial suspensions were dispersed onto a clean silicon wafer, dried, and coated with gold using a sputter coater, then were observed using SEM.

2.16 Plate culture counting method

The treated bacterial suspensions of all groups were diluted, spread on a culture plate, and cultured for 16 h. The number of colonies was then quantified, and the relative survival rate of bacteria was calculated using the following formula:

$$\text{Viability (\%)} = (\text{number of colonies in experimental group} / \text{number of colonies in Control group}) \times 100\%.$$

2.17 Measurement of OD value

To measure the rate of bacterial growth, the treated bacterial suspensions of all groups were cultured for 16 h, and OD600 value were measured to calculate the bacterial concentration, there is a positive correlation between them.

2.18 Zone of inhibition assay

Bacterial suspension (1×10^7 colony-forming units (CFU) per mL) were spread on culture plates, and put TA–GelMA hydrogel, NbC/TA–GelMA hydrogel and NbC/TA–GelMA hydrogel on culture plates, referred to as TA–GelMA hydrogel, NbC/TA–

GelMA hydrogel and NbC/TA–GelMA hydrogel group respectively, the NbC/TA–GelMA hydrogel group received an additional 10 min of NIR irradiation. Meanwhile, we placed drug sensitivity disks of the same size in Control group and NIR group, the NIR group received an additional 10 min of NIR irradiation.

2.19 Cytotoxicity assay *in vitro*

The experiment was divided into four groups, namely the Control group, GelMA hydrogel group, TA–GelMA hydrogel group, and NbC/TA–GelMA hydrogel group. Based on the results of the hydrogel photothermal performance testing, NbC nanoparticles with a concentration of 750 μg mL^{-1} were added in the NbC/TA–GelMA hydrogel group.

We used a CCK-8 kit to evaluate the *in vitro* cytotoxicity of hydrogel extracts on HOK. After sterilization, the hydrogels were placed in 15 mL centrifuge tubes containing 2 mL of DMEM culture medium supplemented with 10% fetal bovine serum, and we obtained the extracts after 24 h. The Control group refers to the culture medium without hydrogel under the same conditions. Meanwhile, 100 μL of HOK suspension containing 1×10^4 cells were added to each well of a 96-well plate and incubated at a constant temperature for 24 h. The culture medium was aspirated, and the cells were washed three times with sterile PBS. Subsequently, 100 μL of the hydrogel extracts of each group and culture medium of the Control group were added to each well for 24 and 48 h. Finally, 10 μL of CCK-8 reagent was added to each well and incubated at a constant temperature for 4 h. The absorbance values of each group were measured at 450 nm using an enzyme-linked immunosorbent assay (ELISA) reader. The cell viability was calculated as follows:

$$\text{Cell viability (\%)} = (\text{OD450 in experimental group/OD450 in Control group}) \times 100\%.$$

2.20 *In vivo* experiments in SD rats

Thirty male SD rats were randomly divided into five groups ($n = 6$ per group): Control group (mucosal impairment group), NIR group (1 W cm^{-2}; 10 min), TA–GelMA hydrogel group, NbC/TA–GelMA hydrogel group, and NbC/TA–GelMA hydrogel (NIR) group. Initially, an oral mucosal impairment model was established in SD rats. After administering anesthesia to eliminate pain and discomfort in the rats, the tongue abdomen mucosa was exposed, and a homemade oral fixation device was used to open the rats' mouths for clear observation. A heated metal rod was then used to contact a specific area of the tongue abdomen mucosa for 5 s, causing physical damage. One day later, successful establishment of the model was confirmed. The Control group received no treatment, the NIR group underwent NIR irradiation on the wound for 10 min. The other three groups were respectively covered with TA–GelMA hydrogel, NbC/TA–GelMA hydrogel, and NbC/TA–GelMA hydrogel on the wound, and NbC/TA–GelMA hydrogel (NIR) group received an additional 10 min of NIR irradiation. We then recorded the condition of the wound and body weight of the rats every two days. On the last day, tissue samples from the impaired areas were collected and sectioned. Hematoxylin–Eosin (H&E) staining and Masson staining were performed on these tissue sections after euthanizing all the SD rats.

2.21 Statistical analysis

SPSS Statistics 25.0 was used to analyze the data. Measures were conformed to normal distribution and data were expressed as the mean ± standard deviation. One-way analysis of variance (ANOVA) and Student's *t*-test (*T*-test) were used, and differences were considered statistically significant at $p < 0.05$.

3 Results and discussion

3.1 Characterization of hydrogel

In this experiment, we first synthesized the hydrogels and characterized their morphology and composition. Fig. 1a depicts an illustration of GelMA hydrogels, TA–GelMA hydrogels and NbC/TA–GelMA hydrogels preparation. The average particle size of NbC nanoparticles in the NbC/TA–GelMA hydrogel was 164.2 nm (Fig. 1b), which would markedly increase the specific surface area, leading to favorable heat absorption and enhancing the efficiency of photothermal conversion. The morphology and composition of the synthesized hydrogels were characterized. Optical images of the hydrogels are shown in Fig. 1c. GelMA hydrogel, TA–GelMA hydrogel, and NbC/TA–GelMA hydrogel were white, yellow, and black, respectively. The mapping results of the NbC/TA–GelMA hydrogel are shown in Fig. 1d, where C, O, and N are common to GelMA and TA, P is an element of LAP, and Nb is a representative element of NbC. SEM showed that the hydrogels were porous (Fig. 1e), and the pore size in the hydrogel scaffold gradually decreased with the addition of TA and NbC step by step, possibly caused by the interaction of the three substances to form a more compact three-dimensional structure. In addition, a uniform distribution of NbC nanoparticles was observed in the hydrogel with NbC added. The XRD results (Fig. 1f) showed that the NbC/TA–GelMA hydrogel has a peak position that matches well with the NbC standard card and the direction of the arrow indicates the characteristic peak of GelMA hydrogel. Collectively, these findings indicated that the NbC/TA–GelMA hydrogel was successfully synthesized.

3.2 Hydrogel adhesion property

As hydrogels are applied in the oral cavity, good adhesion properties are crucial considering the wet and highly dynamic environment.[28] We evaluated the adhesion performance of the hydrogels on rat organs. As shown in Fig. 2a, the heart, liver, spleen, and kidney adhered to the slides *via* the NbC/TA–GelMA hydrogels. The subsequent lap shear experiment of NbC/TA–GelMA hydrogels on fresh porcine gingival mucosa revealed that the adhesion strength increased significantly with the addition of TA and NbC, from 10 kPa to 22 kPa (Fig. 2b). Force–displacement curves of different hydrogels for the lap shear experiment showed that hydrogels with TA and NbC could withstand stronger shear

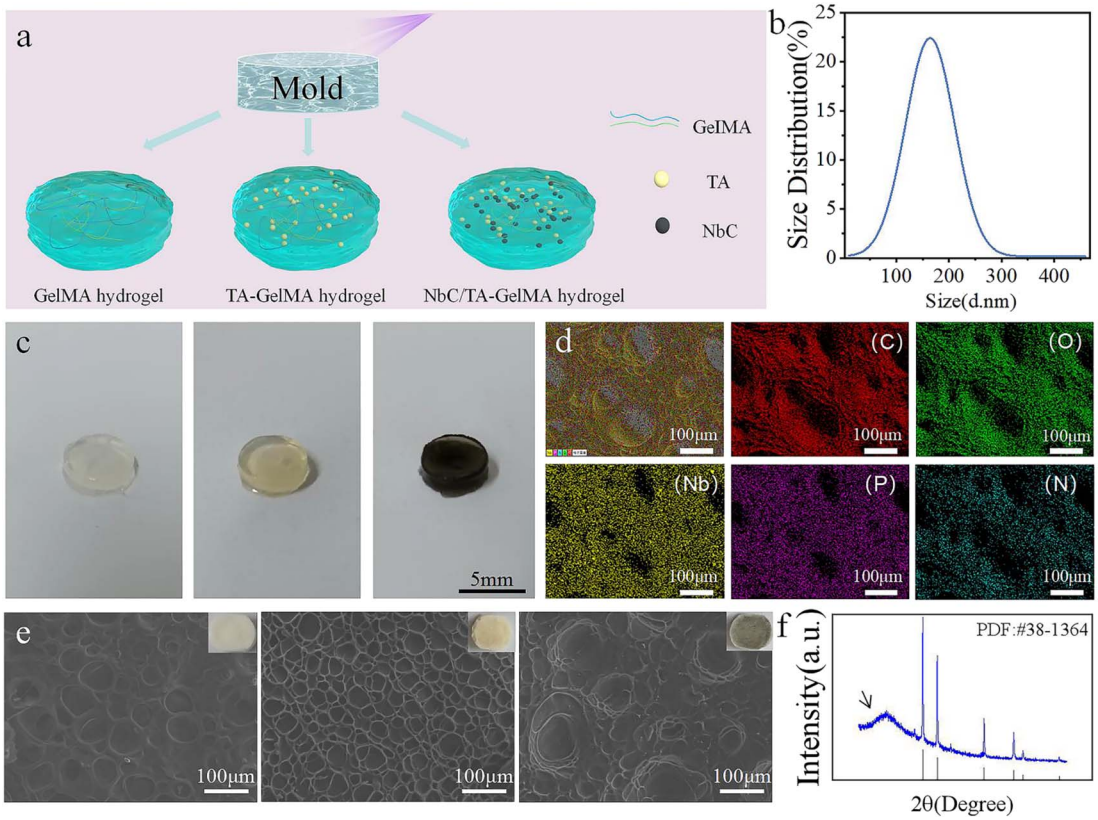

Fig. 1 (a) Preparation of hydrogels. (b) Particle size distribution chart of NbC nanoparticles. (c) Photographs of GelMA hydrogels, TA–GelMA hydrogels, NbC/TA–GelMA hydrogels. (d) C, O, Nb, P and N maps in the SEM image of NbC/TA–GelMA hydrogels. (e) SEM images of GelMA hydrogels, TA–GelMA hydrogels, NbC/TA–GelMA hydrogels. (f) XRD of NbC/TA–GelMA hydrogels.

forces (Fig. S1†). This finding can be attributed to the presence of a catechol-rich group in TA, which provides interfacial adhesion bonding points, thereby enhancing its bonding capacity. For instance, TA can interact with proteins through hydrogen bonding and non-covalent bonding, resulting in a strong adhesion effect.[44] To further validate the adhesive properties of the hydrogels, we conducted a simulated saliva experiment. We observed that the GelMA hydrogels quickly peeled off from the porcine gingival oral mucosa and almost no hydrogel remained. However, after 8 h of magnetic stirring, only one-sixth of the NbC/TA–GelMA hydrogels peeled off (Fig. S2†). In summary, NbC/TA–GelMA hydrogels have good adhesive properties in wet and highly dynamic environments.

3.3 Physical properties of hydrogels

The swelling property of hydrogels can affect the healing of damaged tissues of the oral mucosa and therefore should be considered when using the hydrogels for treatment of oral mucosal impairment.[50–52] Given the tight adhesion of the hydrogels to the oral mucosa, it is important that the hydrogels have low water absorption. As shown in Fig. 2c, the hydrogels with TA and NbC had a lower swelling rate in artificial saliva and got balanced at 4 h. The stability of hydrogels applied in oral mucosal impairments is also a crucial factor. If the degradation of hydrogels is too rapid, the slow release of TA and proliferation of cells will be disrupted, hindering tissue repair. We found that, after 14 days, compared with the degradation rate of the GelMA hydrogel (34.55 ± 2.72%), the NbC/TA–GelMA hydrogel had a lower degradation rate (18.33 ± 1.18%) and reached a stable state by the third day (Fig. 2d). We also examined the mechanical properties of the hydrogels through compressive strength tests. Compared with the 33 kPa of the GelMA hydrogel, the NbC/TA–GelMA hydrogel had a compressive strength of 86 kPa (Fig. 2e), and this stronger compressive strength would be sufficient to withstand the pressure exerted by tissues such as the tongue in the oral cavity. The compressive strength–distance curves of all hydrogels showed a gradual increase, indicating that the hydrogels are flexible and tough (Fig. S3†).

3.4 TA release performance

TA has strong antibacterial and anti-inflammatory properties, and the efficiency of TA release from hydrogels affects the healing process of oral mucosal impairments. We found that the release rate of TA was significantly increased with NIR, reaching 84% after 10 h (Fig. 2f), which would be very beneficial for hydrogels to promote healing of oral mucosal impairments.

3.5 Hemostatic effect

Oral mucosal impairments often lead to early hemorrhage, which can affect the healing process, so the hemostatic effect of

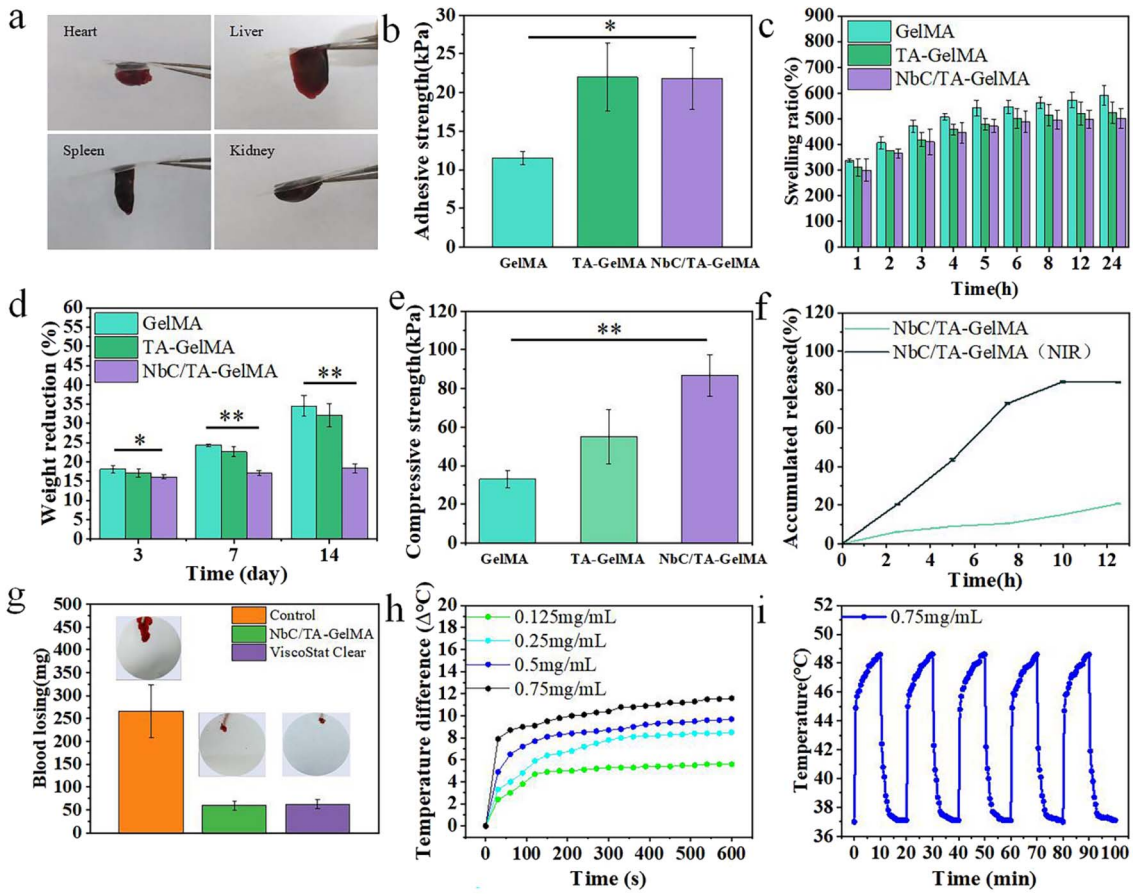

Fig. 2 (a) Photographs of NbC/TA–GelMA hydrogel adhered to the heart, liver, spleen and kidney. (b) Lap shear adhesion abilities of different hydrogels. * represents a statistical significant increase on adhesion abilities for NbC/TA–GelMA hydrogel, compared to GelMA hydrogel ($p < 0.05$). (c) Swelling ratios of GelMA, TA–GelMA, NbC/TA–GelMA hydrogels. (d) Degradation rates of GelMA, TA–GelMA, NbC/TA–GelMA hydrogels. Asterisks represent a significant weight reduction for GelMA hydrogel, compared to NbC/TA-GelMA hydrogel ($p^* < 0.05$, $p^{**} < 0.01$). (e) Compressive strength of GelMA, TA–GelMA, NbC/TA–GelMA hydrogels. ** represents a significant increase on compressive strength for NbC/TA–GelMA hydrogel, compared to GelMA hydrogel ($p < 0.01$). (f) Comparison of TA release performance with and without NIR irradiation. (g) Rat tail amputation with different treatments and corresponding quantification of blood loss. (h) Heating curves of NbC/TA–GelMA hydrogels with different concentrations of NbC. (i) Temperature cycling diagram of NbC/TA–GelMA hydrogel mixed with 0.75 mg mL^{-1}.

the hydrogels is crucial. As shown in Fig. 2g, after the rat's tail was amputated and not coated with anything, a significant amount of blood flowed out onto the filter paper. In contrast, only a small amount of blood flowed out of the severed tails coated with NbC/TA–GelMA hydrogel and ViscoStat Clear, and the NbC/TA–GelMA hydrogel was observed to be tightly bonded to the severed tail surface. Measurements of the amount of bleeding showed that there was only 60 mg in the NbC/TA–GelMA hydrogel group and 62.6 mg in ViscoStat Clear group compared with 266.67 mg in the Control group. In summary, the NbC/TA–GelMA hydrogel has a good hemostatic effect, which could be effective to promote healing of oral mucosal impairments.

3.6 Photothermal property

Materials with good photothermal performance can not only be used for photothermal sterilization, but the mild photothermal effect can also promote vascular repair and proliferation.[53] First, we evaluated the Visible-NIR absorption spectra of different concentrations of NbC and NbC/TA–GelMA hydrogels with different concentrations of NbC. The results showed that NbC at different concentrations and NbC/TA–GelMA hydrogels containing different concentrations of NbC exhibited good optical absorption performance in the near-infrared region of 800–1300 nm. As the solution concentration increased, the absorption values also increased. The hydrogel with 0.75 mg mL^{-1} concentration of NbC showed an absorption value of around 1.5 in the range of 800–1300 nm, demonstrating good optical absorption performance (Fig. S4†). Next, we explored temperature rise effect of different concentrations of NbC. The deionized (DI) water did not warm up significantly after 10 min of NIR irradiation, whereas NbC at 0.5 mg mL^{-1} could be warmed to 52.5 °C after 10 min of NIR irradiation (Fig. S5†). In addition, we used NbC at 0.5 mg mL^{-1} for five temperature-lift cycles, which demonstrated good and stable photothermal performance (Fig. S6†). Furthermore, as shown in Fig. 2h, the hydrogel with 0.75 mg mL^{-1} concentration of NbC could be warmed to 48.6 °C after 10 min of NIR irradiation, and it had stable photothermal

performance (Fig. 2i), which fully met our experimental requirements. The results of the infrared thermal imaging test showed that the temperature of the hydrogel rapidly increased under NIR light irradiation (Fig. S7†).

3.7 Anti-bacterial properties of hydrogels

Given that bacteria can significantly impede the healing of oral mucosa, it is essential that hydrogels possess potent antibacterial properties. In live/dead bacterial staining experiments conducted on *S. aureus*, NbC/TA–GelMA hydrogel group had the majority of red fluorescent dots, indicating that the hydrogel had a marked antibacterial effect (Fig. 3a). We observed from SEM images that bacterial cell membrane rupture and cytoplasmic efflux resulted in mutual adhesion in NbC/TA–GelMA hydrogel group compared with Control group, NIR group, and GelMA hydrogel group, the bacteria in these three groups appeared as grape-like clusters with smooth and intact cell membranes. We also observed morphological damage in some bacteria from the TA–GelMA hydrogel group (Fig. 3b). This could be attributed to the increase in temperature of the NbC/TA–GelMA hydrogel under NIR irradiation, which resulted in the destruction of the bacterial cell wall and membrane, leading to bacterial death.[54,55] The plate culture counting experiment confirmed that TA–GelMA hydrogel group exhibited lower colony counts of *S. aureus* compared with Control group, NIR group, and GelMA hydrogel group, whereas NbC/TA–GelMA hydrogel group had hardly any colonies on the plates (Fig. 3c). The survival rate of *S. aureus* was also determined using the plate culture counting method, and as shown in Fig. 3d, the bacterial survival rate in the NbC/TA–GelMA hydrogel group was only 1.03 ± 0.38%, which was significantly different from the other groups ($p < 0.05$). We evaluated bacterial growth by measuring the OD600 values (Fig. 3e). The OD600 value decreased to 0.25 in TA–GelMA hydrogel group and further reduced to only 0.11 in NbC/TA–GelMA hydrogel group, which was significantly lower than Control group, NIR group, and GelMA hydrogel group ($p < 0.01$). In the zone of inhibition assay, there were almost no inhibition zones in Control group, NIR group, and GelMA hydrogel group, but TA–GelMA hydrogel and NbC/TA–GelMA hydrogel groups exhibited inhibition zones (Fig. S8†).

We found a similar antibacterial effect on *E. coli* as that for *S. aureus* (Fig. 4). The live/dead bacterial staining results for *E. coli*

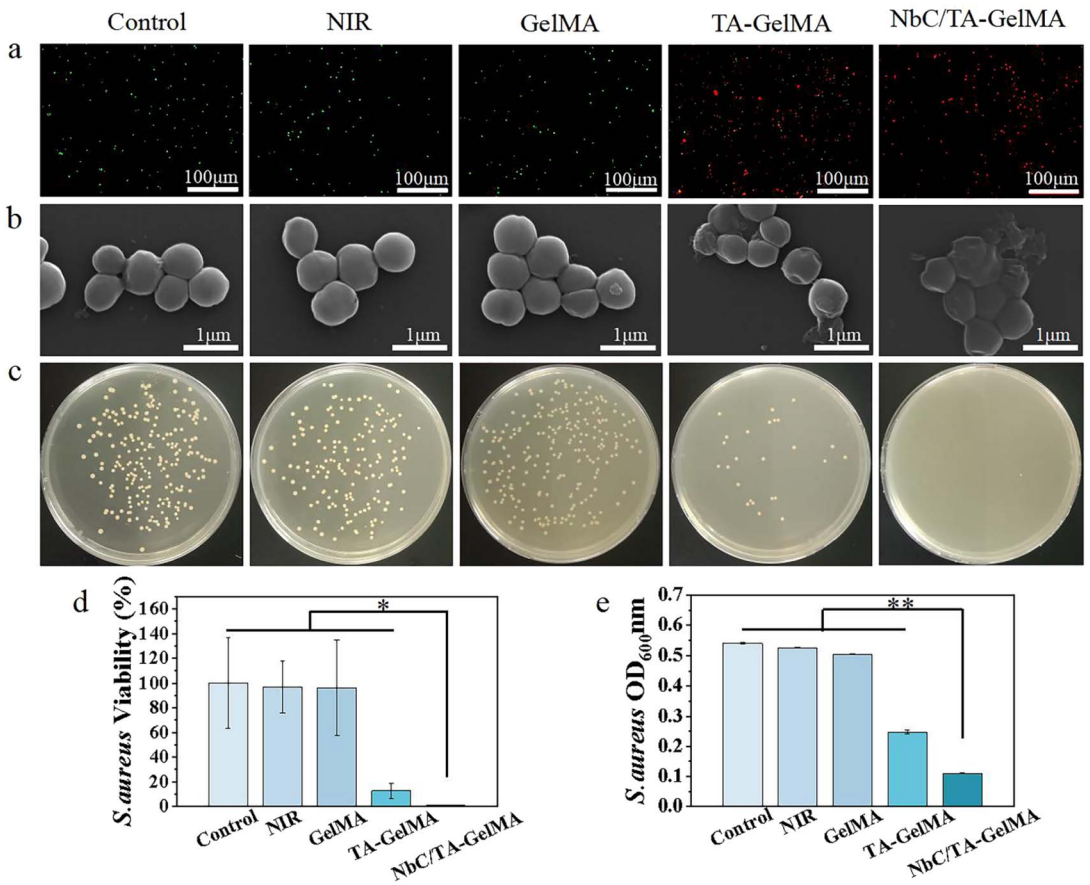

Fig. 3 (a) Live/dead bacterial staining of *S. aureus* of different groups. (b) SEM images of *S. aureus* of different groups. (c) Photos of survival bacteria colonies on agar plates of different groups. (d) Viability ratios of different groups against *S. aureus*. * represents a significant reduction on viability ratios for NbC/TA–GelMA hydrogel group, compared to other groups ($p < 0.05$). (e) The OD600 values of bacterial suspension of different groups. ** represents a significant reduction on OD600 values for NbC/TA–GelMA hydrogel group, compared to other groups ($p < 0.01$).

(Fig. 4a) revealed that Control group, NIR group, and GelMA hydrogel group exhibited predominantly green fluorescent spots. There was a relative increase in red fluorescent spots for TA–GelMA hydrogel group, and NbC/TA–GelMA hydrogel group showed predominantly red fluorescent spots. In the SEM observations of morphological changes of *E. coli* with the hydrogels, Control group, NIR group, and GelMA hydrogel group exhibited a uniform cylindrical shape with no cytoplasmic leakage. In TA–GelMA hydrogel group, some bacterial cell walls had ruptured, resulting in cytoplasmic content leakage and irregular morphological changed, and NbC/TA–GelMA hydrogel group demonstrated a more complete destruction (Fig. 4b). In the plate counting experiment, we saw a decrease in the bacterial colony counts in TA–GelMA hydrogel group compared to Control group, NIR group, and GelMA hydrogel group, whereas NbC/TA–GelMA hydrogel group had almost no colonies (Fig. 4c). We also obtained the relative survival rates of bacteria in each group through plate counting method (Fig. 4d). NbC/TA–GelMA hydrogel group had the lowest survival rate with $0.99 \pm 1.13\%$, which was significantly different from the other groups ($p < 0.05$). In the antibacterial experiment, the OD600 value in NbC/TA–GelMA hydrogel group was 0.18 (Fig. 4e), which was significantly lower than those of the other groups ($p < 0.01$). Our results for the zone of inhibition assay showed that there were almost no inhibition zones in Control, NIR, and GelMA hydrogel groups, but TA–GelMA hydrogel and NbC/TA–GelMA hydrogel groups had inhibition zones (Fig. S9†). In summary, relative to Control group, NIR group, and GelMA hydrogel group, TA–GelMA hydrogel group has some antibacterial effects, whereas NbC/TA–GelMA hydrogel group has superior antibacterial effects. The antibacterial ability of TA is well known,[56,57] and the combination of TA with photothermal sterilization performance of NbC can improve antibacterial effects.

3.8 Evaluation of the healing effect of oral mucosal impairment in SD rats

To further validate the efficacy of the hydrogels, we simulated oral mucosal impairment in SD rats. By the eighth day of the experiment, the wound site treated with NbC/TA–GelMA hydrogel (NIR) had mostly healed, with no significant redness or swelling compared to the Control group (mucosal impairment group). The color and texture of the mucosa at the wound site had returned to normal (Fig. 5a). We quantified the healing

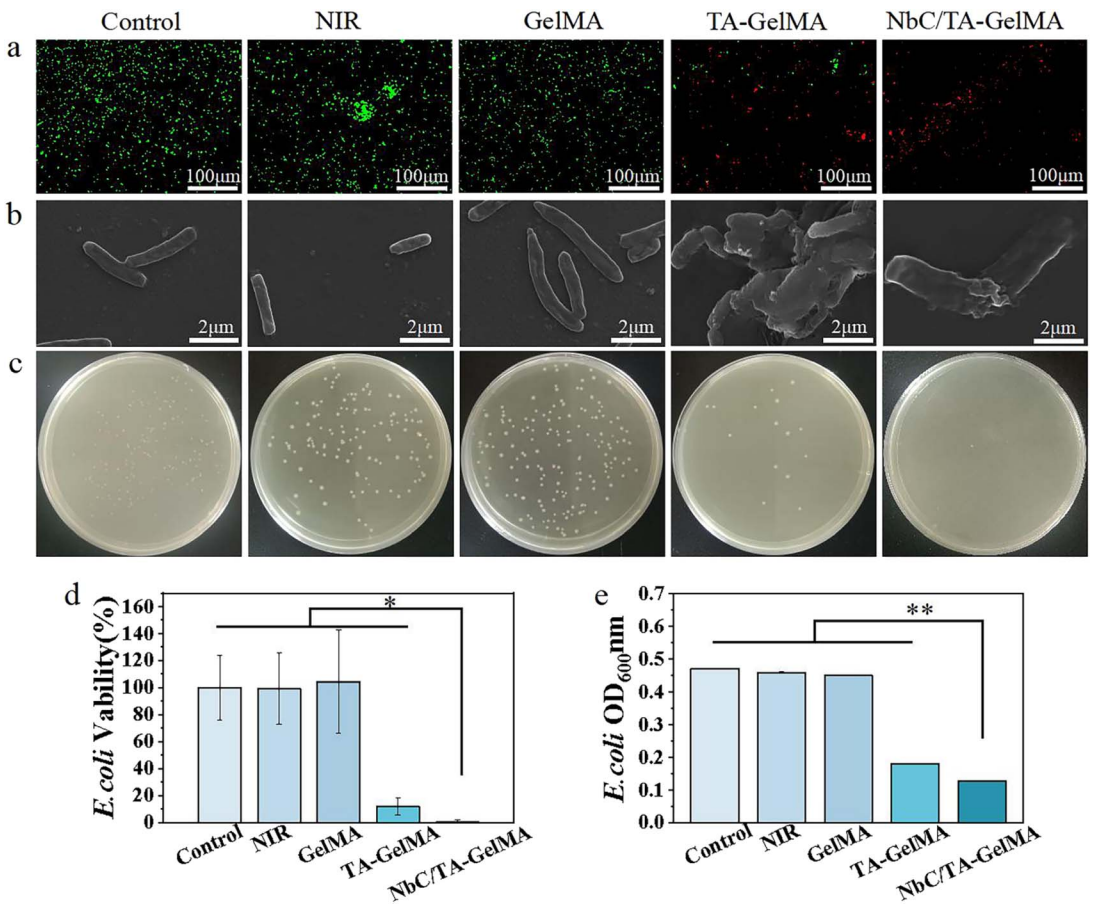

Fig. 4 (a) Live/dead bacterial staining of *E. coli* of different groups. (b) SEM images of *E. coli* of different groups. (c) Photos of survival bacteria colonies on agar plates of different groups. (d) Viability ratios of different groups against *E. coli*. * represents a significant reduction on viability ratios for NbC/TA–GelMA hydrogel group, compared to other groups ($p < 0.05$). (e) The OD600 values of bacterial suspension of different groups. ** represents a significant reduction on OD600 values for NbC/TA–GelMA hydrogel group, compared to other groups ($p < 0.01$).

area of oral mucosal impairment and observed a trend of healing across all groups. By the eighth day, the TA–GelMA hydrogel group (90.59 ± 5.68%) and NbC/TA–GelMA hydrogel group (93.03 ± 5.56%) exhibited distinct therapeutic effects compared with the Control group (78.16 ± 12.77%) and the NIR group (79.75 ± 12.77%). The NbC/TA–GelMA hydrogel (NIR) group showed almost complete healing (99.29 ± 0.87%), emphasizing the efficacy of this treatment in promoting wound closure (Fig. 5b). To assess the safety of the hydrogels *in vivo*, we measured the weights of SD rats, and found no significant difference between all groups (Fig. 5c). This proves that the NbC/TA–GelMA hydrogels did not have obvious acute toxic effects on SD rats. In addition, we conducted cell toxicity testing *in vitro*. As shown in Fig. S10,† the CCK-8 results demonstrated that the cell viability of HOK in all groups remained above 90% at 24 and 48 h and was comparable with that of the Control group. In summary, the hydrogels synthesized in this study demonstrated excellent biocompatibility. We conducted H&E staining and Masson staining on tissues at the site of mucosal impairment in rats to assess the therapeutic effects of the hydrogels from a histopathological perspective. In H&E staining, as shown in Fig. 5d, the Control group showed significant epithelial loss and there was basal layer destruction, disordered cell arrangement, and chronic inflammatory cell infiltration in the epithelium, with abundant deeply stained lymphocytes and plasma cells, which also were found in the NIR group. And re-epithelialization was observed in the NbC/TA–GelMA hydrogel (NIR) group, the inflammation was significantly reduced, with fewer inflammatory cell infiltrates and an intact basal layer. Meanwhile, regeneration of the epithelial tissue with incomplete healing was also observed in the other two groups, and there was an improvement in the inflammatory status compared with the Control group, but this was not as good as in the NbC/TA–GelMA (NIR) hydrogel group. Masson staining also indicated the healing status of the groups, with loose connective tissue and disorganized collagen fibers in the Control group and effective healing in the NbC/TA–GelMA hydrogel (NIR) group (Fig. 5e).

4 Conclusions

In this study, we successfully synthesized and characterized NbC/TA–GelMA hydrogels. Our results show that the NbC/TA–GelMA hydrogel has good wet adhesive properties and compression resistance. These properties contribute to enhanced adhesion of the hydrogel in the moist oral cavity while also providing resistance against potential disruption caused by movement of the tongue. The NbC/TA–GelMA

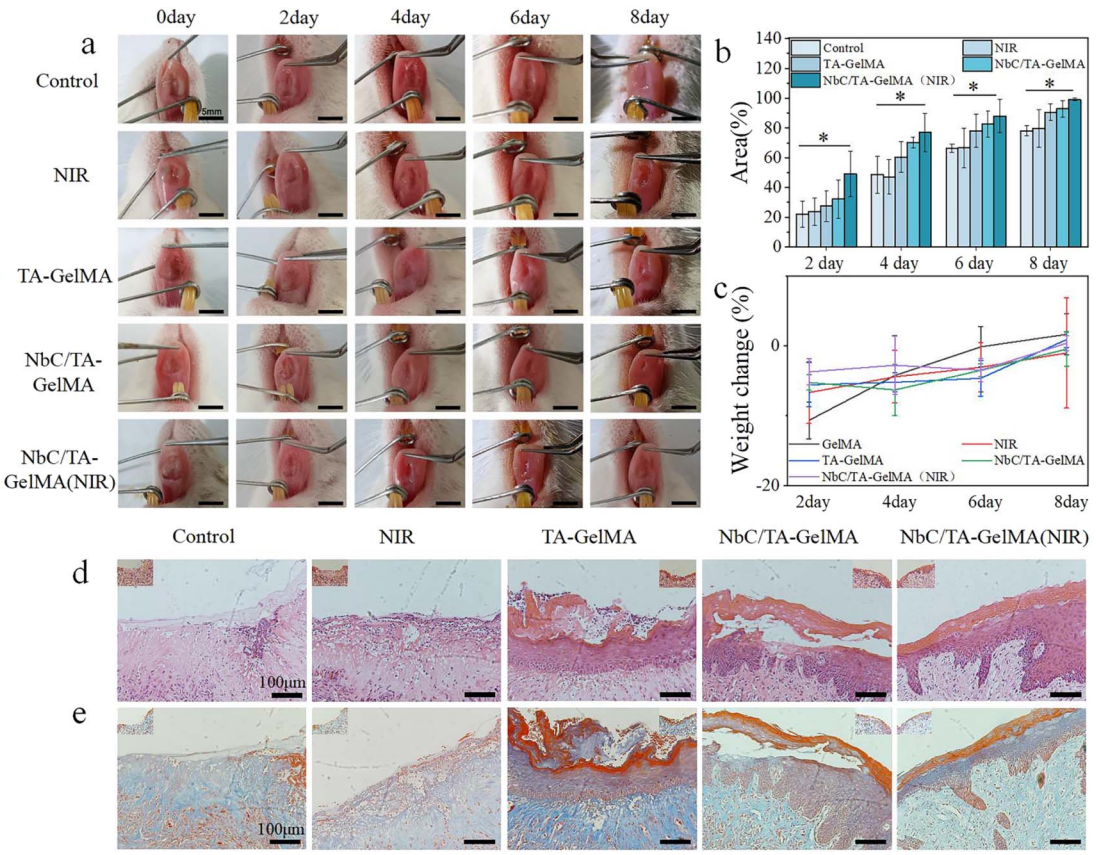

Fig. 5 (a) Photos of oral mucosal impairment in rats treated of different groups. (b) Statistical analysis of healing area for oral mucosal impairment at different times in each group. * represents a significant increase on healing area for NbC/TA–GelMA (NIR) hydrogel group, compared to Control group ($p < 0.05$). (c) Body weight recordings of rats of different groups. (d) H&E staining & (e) Masson staining on the tissues of mucosal impairment in rats.

hydrogel has a low swelling ratio and low degradation rate, which ensure a tighter adhesion of the hydrogel to the oral mucosa and stability of the hydrogel. And the good hemostatic effect indicates that the hydrogel can function as a hemostat early in the impairment, thus preventing the blood from providing nutrients for bacteria. The photothermal effect of the NbC/TA–GelMA hydrogel works synergistically with the antibacterial effect of TA to inhibit bacterial growth and protect the wound from further damage caused by bacteria. The NbC/TA–GelMA hydrogel exhibits efficient release of TA, and its anti-inflammatory properties are particularly advantageous in the later stages of wound recovery. In addition, the NbC/TA–GelMA hydrogel has no significant cytotoxicity, which is crucial for clinical applications. All these properties are conducive to the creation of a suitable microenvironment for oral mucosal impairment healing and promote the healing of oral mucosal impairments to a certain extent. Our experiments *in vivo* further showed that the NbC/TA–GelMA hydrogel could promote the healing of oral mucosal impairments in rats. The tissue staining showed that the inflammation state of the NbC/TA–GelMA(NIR) hydrogel group was significantly reduced, which may be attributed to the anti-inflammatory effect of TA. In addition, bacterial infection is one of the causes of inflammation, the photothermal antibacterial effect of NbC could further improve the inflammatory state. In conclusion, this study offers a novel approach for treating oral mucosal impairments, which holds a great clinical significance.

Author contributions

Chen and Yunyu Ren: methodology, validation, investigation, formal analysis, writing – original draft. Lin Zhang and Narisu Hu: conceptualization, project administration. Yingjie Wu and Fang Zhao: writing – review & editing.

Conflicts of interest

There are no conflicts to declare.

Acknowledgements

This work was supported by Heilongjiang Provincial Natural Science Foundation of China (Grant No. YQ2022B005); Fundamental Research Funds for the Central Universities (Grant No. HIT.OCEF. 2023033); China Postdoctoral Science Foundation funded project (Grant No. 2019M651270 and No. 2019T120277); National Natural Science Foundation of China (Grant No. 51972087); Heilongjiang Provincial Natural Science Foundation of China (Grant No. LH2022H043).

References

1 H. An, Z. Gu, L. Zhou, S. Liu, C. Li, M. Zhang, Y. Xu, P. Zhang and Y. Wen, *Acta Biomater.*, 2022, **149**, 126–138.
2 J. J. Soojeong Choi, Y. Bae, Y. Hwang and S.-W. Cho, *Adv. Funct. Mater.*, 2023, **33**, 2303043.
3 F. Laffleur and M. Egeling, *J. Drug Delivery Sci. Technol.*, 2020, **58**, 101839.
4 A. H. M. Al-Rudayni, D. Gopinath, M. K. Maharajan and R. K. Menon, *Transl. Cancer Res.*, 2020, **9**, 3126–3134.
5 J. Kumar, S. L. Teoh, S. Das and P. Mahakknaukrauh, *Front. Physiol.*, 2017, **8**, 00693.
6 X. Li, K. M. Kolltveit, L. Tronstad and I. Olsen, *Clin. Microbiol. Rev.*, 2000, **14**, 547–558.
7 X. Zeng, X. Jin, L. Zhong, G. Zhou, M. Zhong, W. Wang, Y. Fan, Q. Liu, X. Qi, X. Guan, Z. Yan, X. Shen, Y. Wu, L. Fan, Z. Wang, Y. He, H. Dan, J. Yang, H. Wang, D. Liu, H. Feng, K. Jiao and Q. Chen, *Int. J. Oral Sci.*, 2022, **14**, 28.
8 Z. Luo, K. Xue, X. Zhang, J. Y. C. Lim, X. Lai, D. J. Young, Z.-X. Zhang, Y.-L. Wu and X. J. Loh, *Biomater. Sci.*, 2020, **8**, 1364–1379.
9 J. R. Naglik, A. K. nig, B. Hube and S. L. Gaffen, *Curr. Opin. Microbiol.*, 2017, **40**, 104–112.
10 S. Alghamdi, *Saudi J. Biol. Sci.*, 2022, **29**, 318–323.
11 H. Sun, Y. Wang, T. He, D. He, Y. Hu, Z. Fu, Y. Wang, D. Sun, J. Wang, Y. Liu, L. Shu, L. He, Z. Deng and X. Yang, *J. Nanobiotechnol.*, 2021, **19**, 304.
12 M. K. Al-Omiri, J. Karasneh, M. M. Alhijawi, A. M. A. Zwiri, C. Scully and E. Lynch, *J. Oral Pathol. Med.*, 2014, **44**, 278–283.
13 L. Samaranayake and V. H. Matsubara, *Dent. Clin. North Am.*, 2017, **61**, 199–215.
14 M. Motamedifar, N. Tanideh, M. Mardani, B. Daneshvar and M. Hadadi, *Photodermatol., Photoimmunol. Photomed.*, 2020, **37**, 115–122.
15 P. L. Molyneaux, M. J. Cox, S. A. G. Willis-Owen, P. Mallia, K. E. Russell and A. M. Russell, *Am. J. Respir. Crit. Care Med.*, 2014, **190**, 906–913.
16 M. Baym, L. K. Stone and R. Kishony, *Science*, 2016, **351**, 3239.
17 P. Domingo-Calap and J. Delgado-Martínez, *Antibiotics*, 2018, **7**, 7030066.
18 G. Ferro, F. Guarino, A. Cicatelli and L. Rizzo, *J. Hazard. Mater.*, 2017, **323**, 426–433.
19 W. Yu, S. Zhan, Z. Shen, Q. Zhou and D. Yang, *Chem. Eng. J. (Lausanne)*, 2017, **313**, 836–846.
20 J. Bengtsson-Palme and D. G. J. Larsson, *Nat. Rev. Microbiol.*, 2015, **13**, 116–123.
21 J. H. Ryu, J. S. Choi, E. Park, M. R. Eom, S. Jo, M. S. Lee, S. K. Kwon and H. Lee, *J. Controlled Release*, 2020, **317**, 57–66.
22 M. Durán-Lobato, Z. Niu and M. J. Alonso, *Adv. Mater.*, 2019, **32**, 1901935.
23 W. Qi, N. Dong, L. Wu, X. Zhang, H. Li, H. Wu, N. Ward, J. Yu, H. Liu, J. Wang, X. Deng and R. C. Zhao, *Bioact. Mater.*, 2023, **23**, 53–68.
24 H. E. Colley, Z. Said, M. E. Santocildes-Romero, S. R. Baker, K. D'Apice, J. Hansen, L. S. Madsen, M. H. Thornhill, P. V. Hatton and C. Murdoch, *Biomaterials*, 2018, **178**, 134–146.
25 M. M. Hasani-Sadrabadi, P. Sarrion, N. Nakatsuka, T. D. Young, N. Taghdiri, S. Ansari, T. Aghaloo, S. Li, A. Khademhosseini, P. S. Weiss and A. Moshaverinia, *ACS Nano*, 2019, **13**, 3830–3838.

26 S. K. Boda, N. G. Fischer, Z. Ye and C. Aparicio, *Biomacromolecules*, 2020, **21**, 4945–4961.
27 S. Hu, X. Pei, L. Duan, Z. Zhu, Y. Liu, J. Chen, T. Chen, P. Ji, Q. Wan and J. Wang, *Nat. Commun.*, 2021, **12**, 1689.
28 J. Xu, S. Strandman, J. X. X. Zhu, J. Barralet and M. Cerruti, *Biomaterials*, 2015, **37**, 395–404.
29 C. Cavallari, P. Brigidi and A. Fini, *Int. J. Pharm.*, 2015, **496**, 593–600.
30 Y. Wang, Z. Pan, J. Cui, X. Zhang, D. Li, H. Sun, B. Yang and Y. Li, *Acta Biomater.*, 2024, **178**, 68–82.
31 E. Park, J. Lee, K. M. Huh, S. H. Lee and H. Lee, *Adv. Healthcare Mater.*, 2019, **8**, 1900275.
32 Z. Lin, C. Gao, D. Wang and Q. He, *Angew. Chem., Int. Ed.*, 2021, **60**, 8750–8754.
33 G. Begić, M. Petković Didović, S. Lučić Blagojević, I. Jelovica Badovinac, J. Žigon, M. Perčić, O. Cvijanović Peloza and I. Gobin, *Int. J. Mol. Sci.*, 2022, **23**, 2983.
34 L. Sedghi, V. DiMassa, A. Harrington, S. V. Lynch and Y. L. Kapila, *Periodontol. 2000*, 2021, **87**, 107–131.
35 R. M. Logan, A. R. Al-Azri, P. Bossi, A. M. Stringer, J. K. Joy, Y. Soga, V. Ranna, A. Vaddi, J. E. Raber-Durlacher, R. V. Lalla, K. K. F. Cheng and S. Elad, *Support. Care Cancer*, 2020, **28**, 2485–2498.
36 M. E. A. de Kraker, A. J. Stewardson and S. Harbarth, *PLoS Med.*, 2016, **13**, e1002184.
37 X. Wang, F. Lv, T. Li, Y. Han, Z. Yi, M. Liu, J. Chang and C. Wu, *ACS Nano*, 2017, **11**, 11337–11349.
38 M. Xuan, Z. Wu, J. Shao, L. Dai, T. Si and Q. He, *J. Am. Chem. Soc.*, 2016, **138**, 6492–6497.
39 M. Xuan, J. Shao, C. Gao, W. Wang, L. Dai and Q. He, *Angew. Chem., Int. Ed.*, 2018, **57**, 12463–12467.
40 Y. Liu, T. Li, M. Sun, Z. Cheng, W. Jia, K. Jiao, S. Wang, K. Jiang, Y. Yang, Z. Dai, L. Liu, G. Liu and Y. Luo, *Acta Biomater.*, 2022, **146**, 37–48.
41 Z. Jia, X. Lv, Y. Hou, K. Wang, F. Ren, D. Xu, Q. Wang, K. Fan, C. Xie and X. Lu, *Bioact. Mater.*, 2021, **6**, 2676–2687.
42 H. Liu, Q. Li, Y. Xu, Y. Sun, X. Fan, H. Fang, B. Hu, L. Huang, L. Liao and X. Wang, *Biomater. Sci.*, 2023, **11**, 3180–3196.
43 E. Izumi, N. Tanahash, S. Kinugasa, S. Hidaka, N. Zaima and T. Moriyama, *Int. J. Mol. Sci.*, 2022, **23**, 3933.
44 Z. Jia, X. Lv, Y. Hou, K. Wang, F. Ren, D. Xu, Q. Wang, K. Fan, C. Xie and X. Lu, *Bioact. Mater.*, 2021, **6**, 2676–2687.
45 C. Tong, X. Zhong, Y. Yang, X. Liu, G. Zhong, C. Xiao, B. Liu, W. Wang and X. Yang, *Biomaterials*, 2020, **243**, 119936.
46 H. Wang, S. Zhou, L. Guo, Y. Wang and L. Feng, *ACS Appl. Mater. Interfaces*, 2020, **12**, 39685–39694.
47 A. I. V. D. Bulcke, B. Bogdanov, N. D. Rooze, E. H. Schacht, M. Cornelissen and H. Berghmans, *Biomacromolecules*, 2000, **1**, 31–38.
48 A. Erdem, M. A. Darabi, R. Nasiri, S. Sangabathuni, Y. N. Ertas, H. Alem, V. Hosseini, A. Shamloo, A. S. Nasr, S. Ahadian, M. R. Dokmeci, A. Khademhosseini and N. Ashammakhi, *Adv. Healthcare Mater.*, 2020, **9**, 201901794.
49 M. Li, Z. Zhang, Y. Liang, J. He and B. Guo, *ACS Appl. Mater. Interfaces*, 2020, **12**, 35856–35872.
50 Y. Yang, J. Yuan, Y. Ni, Y. Gu, J. Zhou, W. Yuan, S. Xu, L. Che, S. Y. Zheng, W. Sun, D. Zhang and J. Yang, *Composites, Part B*, 2022, **243**, 110119.
51 H. Kamata, K. Kushiro, M. Takai, U. i. Chung and T. Sakai, *Angew. Chem., Int. Ed. Engl.*, 2016, **55**, 9282–9286.
52 Y. Zhan, W. Fu, Y. Xing, X. Ma and C. Chen, *Mater. Sci. Eng., C*, 2021, **127**, 112208.
53 Y. V. Stepanov, I. Golovynska, S. Golovynskyi, L. V. Garmanchuk, O. Gorbach, L. I. Stepanova, N. Khranovska, L. I. Ostapchenko, T. Y. Ohulchanskyy and J. Qu, *J. Photochem. Photobiol., B*, 2022, **227**, 112388.
54 M.-C. Wu, A. R. Deokar, J.-H. Liao, P.-Y. Shih and Y.-C. Ling, *ACS Nano*, 2013, **7**, 1281–1290.
55 M. J. Hajipour, K. M. Fromm, A. A. Ashkarran, D. J. d. Aberasturi, I. R. d. Larramendi, T. Rojo, V. Serpooshan, W. J. Parak and M. Mahmoudi, *Trends Biotechnol.*, 2013, **31**, 61–62.
56 A. Schestakow and M. Hannig, *Biomolecules*, 2020, **10**, 1315.
57 J. Guo, W. Sun, J. P. Kim, J. Guo, W. Sun, J. P. Kim, X. Lu, Q. Li, M. Lin, O. Mrowczynski, E. B. Rizk, J. Cheng, G. Qian and J. Yang, *Acta Biomater.*, 2018, **72**, 35–44.